Heliyon 9 (2023) e17266

Contents lists available at ScienceDirect

Heliyon

journal homepage: www.cell.com/heliyon

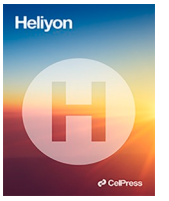

# GEO data mining identifies potential immune-related genes in hypertrophic scar and verities in a rabbit model

Hong Cai [a,b,c,1], Xuan Liu [d,1], Dingbin Liu [e], Bin Liu [f,*]

[a] Department of Dermatology, Air Force Medical University Air Force Medical Center, Beijing, 100142, China
[b] Air Force Clinical College, Anhui Medical University Beijing, 100142, China
[c] The Fifth School of Clinical Medicine, Anhui Medical University, Hefei, 230032, Anhui Province, China
[d] Department of Surgery, Central Medical Branch of PLA General Hospital, Beijing, 100120, China
[e] State Key Laboratory of Medicinal Chemical Biology, Research Center for Analytical Sciences, Tianjin Key Laboratory of Molecular Recognition and Biosensing, College of Chemistry, Nankai University, Tianjin, 300071, China
[f] .Cancer Research Center, Beijing Chest Hospital, Capital Medical University/Beijing Tuberculosis and Thoracic Tumor Research Institute, Beijing, 101149, China

ARTICLE INFO

*Keywords:*
Hypertrophic scar
Immune
Gene expression
Bioinformatics analysis
Animal model

ABSTRACT

*Objective:* Hypertrophic scar (HTS), the secondary major abnormal tissue after wound healing, is the most frequent and severe type of skin scar. Dysregulated immune response plays an important role in HTS formation. In this study, we identified the potential immune-related genes in HTS and explored their potential therapeutic significance.
*Methods:* We first screened out the potential immune-related genes in HTS microarrays via bioinformatics analysis using public datasets. We then constructed a rabbit model of ear scar to investigate the morphological features of HTS and verify the basic expression of potential immune-related genes in HTS tissue. Finally, we used AlphaFold to determine the protein homology between human and rabbit scar tissues.
*Results:* Bioinformatics analysis revealed 22 differentially expressed genes (DEGs) and a single differential infiltration of immune cells (naïve B cells) in HTS and normal tissues. Six of the DEGs were correlated with naïve B cell numerically. CCL2, PLXDC2 and FOXF2 were expressed in rabbit ear scar model. PLXDC2 and FOXF2 showed relatively high homology between human and rabbit scar tissues.
*Conclusions:* PLXDC2 and FOXF2, both closely related to immune cell infiltration and specifically expressed in HTS, represent potential therapeutic targets in HTS.

## 1. Introduction

Damaged cutaneous tissue can be replaced with abnormal connective tissue during tissue regeneration to generate a specific structure known as a scar [1]. Scar can be divided into hypertrophic scar (HTS), keloid scar and atrophic scar [2]. HTS affects people aesthetically, causes itching and pain, and even results in serious distress in their daily lives [3]. The mechanisms underlying HTS genesis include abnormal expression of matrix metalloproteinases in extracellular matrix (ECM), which results in hyperactive

* Corresponding author.
*E-mail address:* liubin@ccmu.edu.cn (B. Liu).
[1] Contributed equally.

https://doi.org/10.1016/j.heliyon.2023.e17266
Received 16 November 2022; Received in revised form 2 June 2023; Accepted 12 June 2023
Available online 14 June 2023

fibroblasts and myofibroblasts [4]. Current guidelines recommend use of silicone sheets and gel as the first line of defense in preventing and treating HTS [5]. However, they are associated with an increased risk of hypopigmentation, contact dermatitis, telangiectasias, and skin atrophy [6]. Therefore, more effective HTS therapies are required, especially for patients with severe HTS.

Recently, biological therapy has been utilized to treat multiple clinical disorders. Products derived from living organisms are emerging as a viable option to prevent and treat diseases. A growing number of theoretical and experimental studies involving scar have shown that the scar microenvironment differs completely from the normal tissue environment, and the changing gene expression plays an important role in scar formation [7–11]. Can the scar formation be improved by altering the gene expression profile locally in the scar tissue?

In the present study, using bioinformatics methods, we screened differentially expressed genes (DEGs) between HTS and normal skin tissue based on published microarray data, and verified DEGs via experimental analysis in an animal model of skin wounds. The aim of this study is to identify the key genes underlying HTS formation, which serve as potential therapeutic regulators in HTS.

## 2. Method

### 2.1. Raw data

The GEO data sets of HTS were selected and only one data set (GSE136906) was obtained as of September 2021 (including 6 patients with normotrophic scar and matched control tissues) [12]. The screening criteria were as follows: mRNA transcriptome dataset of scars obtained from trauma, matching normotrophic scar tissue and its normal tissue, and absence of genetic or immune treatments. As only one dataset was selected, the normalization process was omitted.

### 2.2. Identification and analysis of DEGs

The limma package in R was used to analyze the data. The cutoffs are as follows: Fold change $< -1$ or $>1$, and adj,$P < 0.05$. The limma package and pheatmap were used to generate the heatmaps and volcano plots. Functional analyses of DEGs were performed with "clusterProfiler" and "org.Hs.eg.db", which are used to analyze Gene ontology (GO) and Kyoto Encyclopedia of Genes and Genomes (KEGG).

### 2.3. Construction of protein-protein interaction (PPI) network

Analysis of functional interactions between proteins was conducted using the Search Tool for Retrieval of Interacting Genes/Proteins (STRING) database [13].

### 2.4. Identification of infiltrating immune cells

We used CIBERSORT to estimate the infiltrating immune cells in HTS computationally [14]. The infiltrating immune cells are displayed in a barplot. Heatmaps were generated with "pheatmap", and correlation heatmaps were created using "corrplot". Wilcoxon rank-sum tests were used to analyze the differential distribution of infiltrating immune cells in control and HTS tissues.

### 2.5. Identification of potential immune-related DEGs

Multiple linear regression analysis was used to identify potential immune-related DEGs in infiltrating immune cells and HTS. The infiltrating immune cells with different distribution were entered as dependent variable and DEGs as independent variables. A predictive factor analysis of differential distribution of infiltrating immune cells was conducted via least-squares regression. Based on accuracy as well as computational efficiency, significance was set as follows: absolute value of correlation coefficient greater than 0.5 and p value less than 0.05. Genes selected for this study were labeled as potential immune-related DEGs.

### 2.6. Construction of rabbit ear scar model

We used New Zealand white rabbit (Beijing Jinmuyang Experimental Animal Breeding Co. LTD) to construct the rabbit model of ear scar. The rabbits were 2–3 months of age and weighed 2–2.5 kg each. Rabbits were deeply anesthetized with 1% sodium pentobarbital (3 mL/kg). Drill bits with 10 mm ring were used to compress the ventral side of the rabbit's ear. Subcutaneous tissues and periosteal membranes were mechanically removed with forceps. The bleeding was immediately stopped via slight compression with a sterile gauze. After 30 days, biopsies were obtained from the scar and the surrounding normal tissue. The Ethics Committee of Air Force Medical Center PLA approved the study design protocol (2022-110-YJ01). The research protocol complies with the relevant regulations on ethics and welfare of experimental animals.

### 2.7. Masson's trichrome and HE staining

The scar and the surrounding normal tissue were dehydrated, embedded in paraffin, and cut into 3-μm-thick sections with a paraffin slicer. Masson's trichrome or HE was used to stain the dewaxed paraffin sections and observed under a microscope. A blue

signal indicated positive staining for collagen.

### 2.8. Verification of potential immune-related DEGs by qPCR

The qPCR assay was performed with an ABI StepOnePlus Real-time PCR System (ABI-7500, Applied Biosystems) and PowerUp SYBE Green Master Mix Kit (Cat. A25741, Applied Biosystems). The qPCR primers used were as follows:

CCL2-F: 5′- ACCAACTCAGAAGCTGCCGTC-3′; CCL2-R: 5′- CTTTGGGACACTTGGTGCTGTT-3′;
PLXDC2-F: 5′- TGGACTCACACGCCTACAGC-3′; PLXDC2-R: 5′- CTGAGTGTTGTTGTCCTGCCCA-3′;
FOXF2-F: 5′- GAAGAACTCGGTGCGCCACAAC-3′; FOXF2-R: 5′- CCTCCTCGAACATGAACTCGCT-3′;
GAPDH-F: 5′- CAGCCTGAACCTGTGCCAGAAC -3′; GAPDH-R: 5′- GTCCGTTCTTGTACTCCACGCT-3′.

### 2.9. Prediction of protein structure by AlphaFold

We downloaded human and rabbit protein sequences from NCBI and input them into AlphaFold program. The number_recycles and num_moldels were set at 3 and 5, respectively. We selected the highest score one in the study.

### 2.10. Statistical analysis

The Wilcoxon rank-sum test was performed using GraphPad Prism with normally distributed data. A P value of less than 0.05 was deemed significant.

## 3. Results

### 3.1. Identification of DEGs or lncRNAs from the selected dataset

Our screening criteria resulted in the selection of a single data set for this study. This data set downloaded from GEO contained 6 paired samples. Statistically significant difference was defined as $P < 0.05$ and a fold change >10 between the HTS and normal control

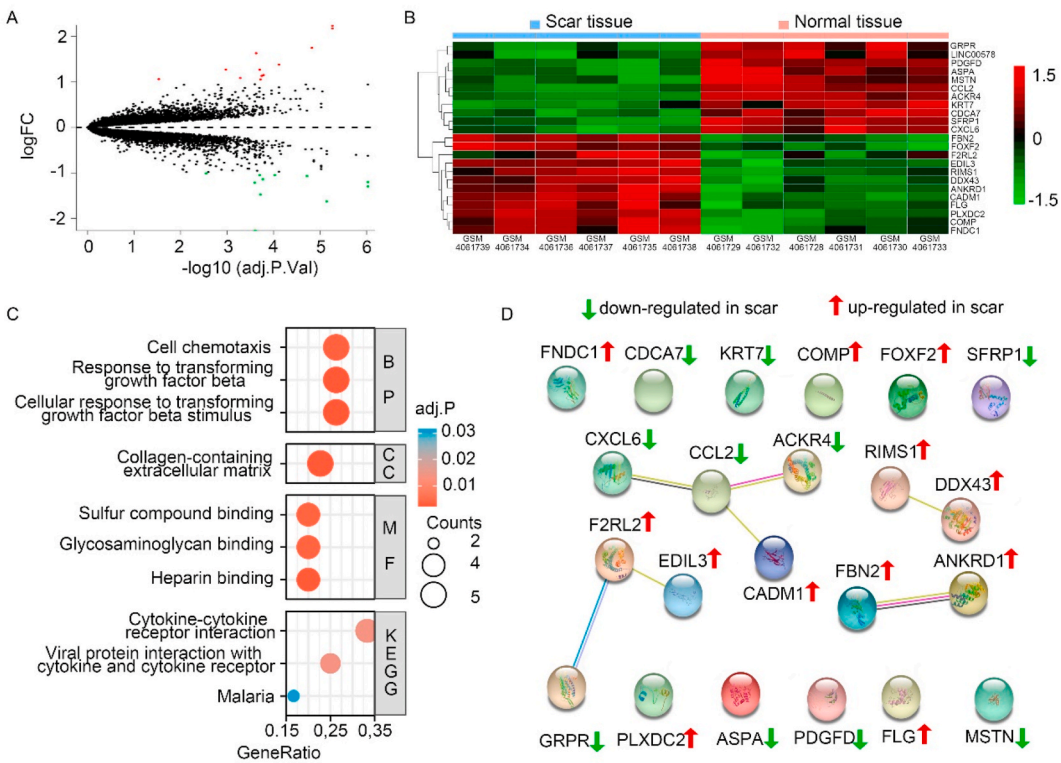


**Fig. 1.** Identification and analysis of DEGs between HTS and normal tissues. (A) Scatterplot shows higher or lower expression of DEGs between the HTS and normal tissue samples; (B) Heatmap shows the expression of genes between HTS and normal tissue samples; (C) GO and KEGG analyses of DEGs; (D) The PPI network of DEGs.

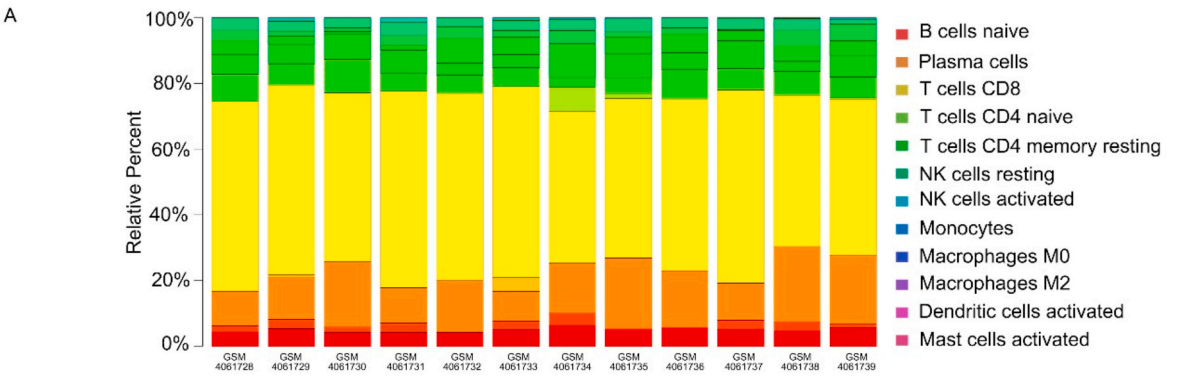


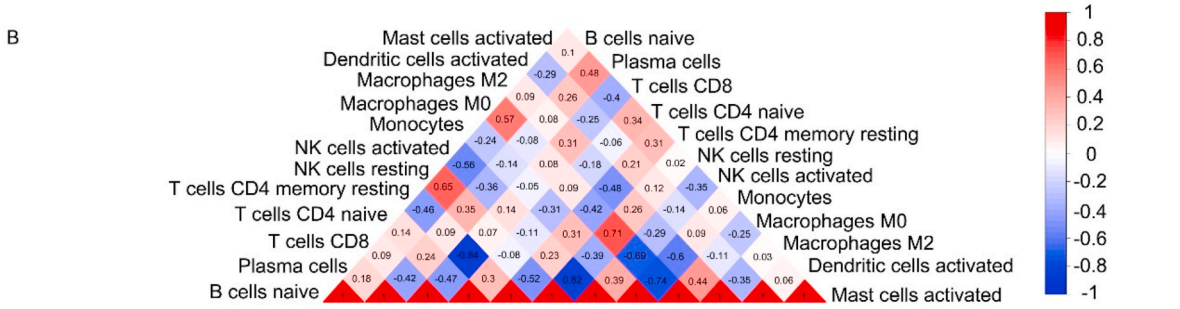


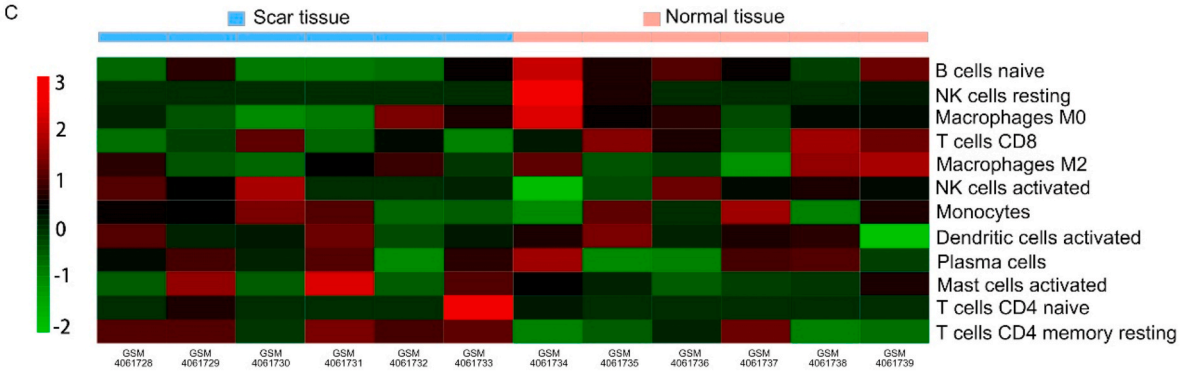


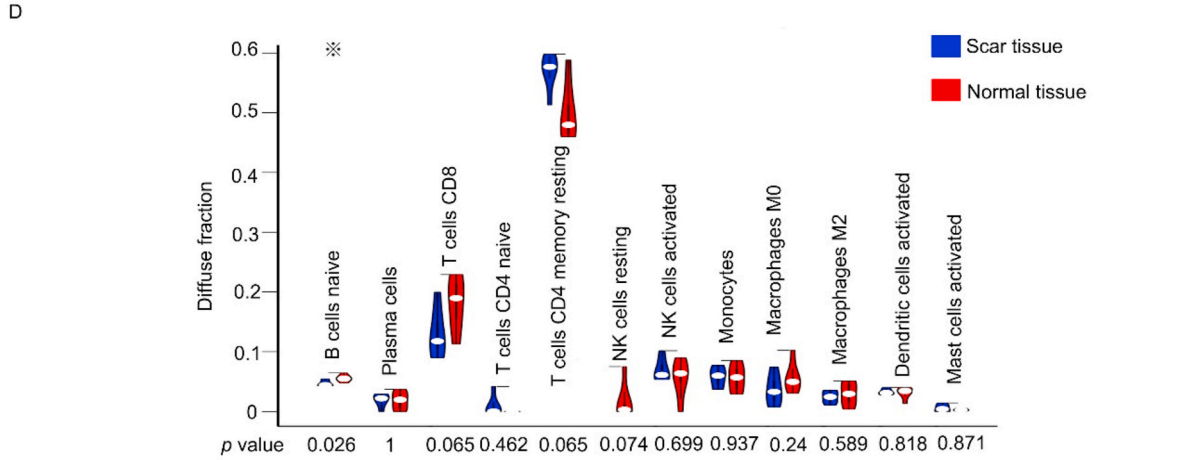


*(caption on next page)*

**Fig. 2.** Different distribution of immune cells between HTS and normal tissues. (A) Histogram shows the distribution status in each HTS and normal tissue sample; (B) The correlation between immune cells in HTS and normal tissues; (C) Violin diagram shows the difference in distribution between HTS and normal tissues. * denotes p value < 0.05.

samples. A total of 23 DEGs or lncRNAs were identified from more than 10,000 genes and lncRNAs. The results revealed that 12 out of the DEGs were highly expressed, whereas the remaining 10 DEGs and 1 differential expressed lncRNA were down-regulated in HTS (Fig. 1A and B). Due to the lack of DEGs in this screen, the upregulated and downregulated pathways were enriched via GO and KEGG pathways. The results showed that those DEGs were enriched in multiple components, such as cell chemotaxis, response to transforming growth factor beta, and collagen-containing extracellular matrix (Fig. 1C).

### 3.2. Protein-protein interaction (PPI) network construction

We analyzed the functional interactions between DEGs using the STRING database. A total of 11 genes, including CXCL6, CCL2, ACKR4, CADM1, RIMS1, DDX43, FBN2, ANDKRD1, GRPR, F2RL2 and EDIL3 were identified in 4 pairs of interacting networks (Fig. 1D).

### 3.3. Differences based on the distribution of B naïve cells between HTS and normal tissue

The CIBERSORT algorithm estimates the proportion of tumor-infiltrating immune cells in tumor microenvironments. In this study, we used it to estimate the infiltrating immune cells in HTS. We found that the proportion of different infiltrating immune cells was roughly similar to individual variations (Fig. 2A and B). There was no significant correlation between their numerical values in either HTS or normal tissues (Fig. 2C). Using the Mann-Whitney rank-sum test, we calculated differences in immune cell distribution infiltration. We found a significant difference in the distribution of B naïve cells between HTS and normal tissues (Fig. 2D).

### 3.4. Statistical correlations between DEGs and differentially distributed immune cells

We used Pearson correlation to analyze the numerical correlation between 23 DEGs and B naïve cells. We found that six DEGs (CCL2, CDCA7, ACKR4, PLXDC2, FOXF2 and CADM1) showed statistical correlation with B naïve cells in HTS. The absolute value of correlation coefficient was greater than 0.5 and the p value was less than 0.05 (Fig. 3A–F). Three of the six genes showed higher correlation coefficient (greater than 0.6) but no studies involving HTS were reported. We named them potential immune-related DEGs.

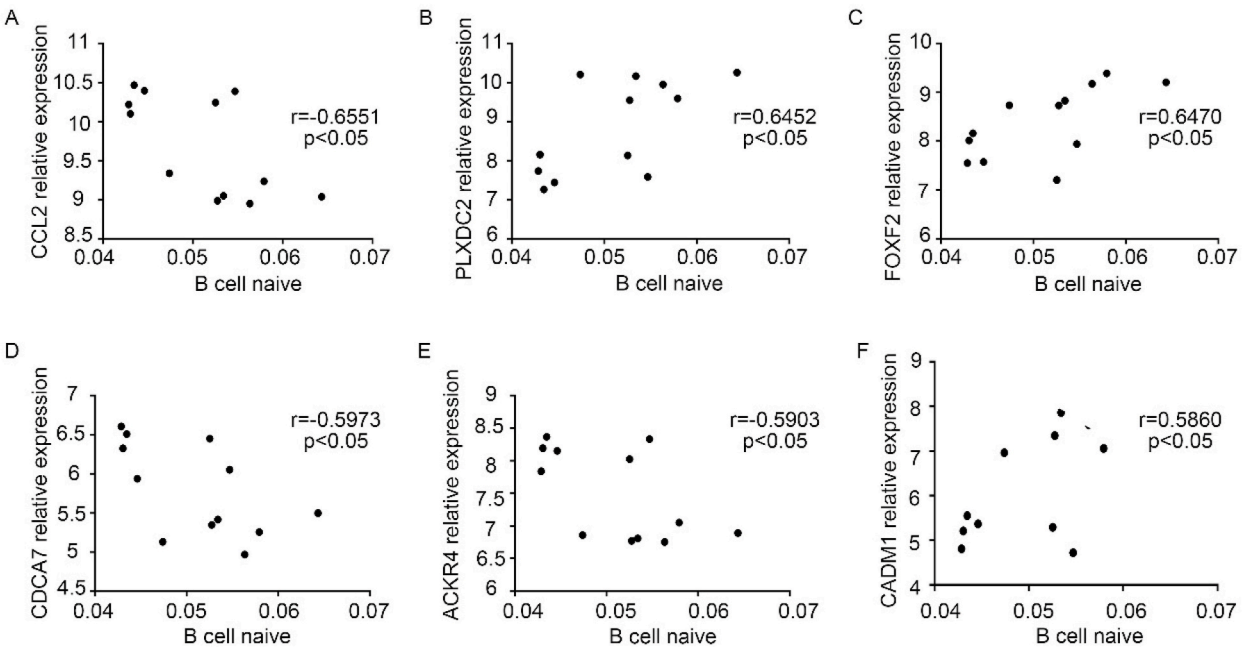


**Fig. 3.** DEGs showing moderate correlation with naïve B cells, which represent the differentially distributed immune cells between HTS and normal tissues. (A to F) Scatter plots of correlation analysis between naïve B cells and CCL2, PLXDC2, FOXF2, CDCA7, ACKR4 and CADM1 expression.

### 3.5. Verification of potential immune-related DEGs in a rabbit model of HTS

Due to the lack of established cell lines of HTS, we constructed an HTS model of rabbit ear (Fig. 4A). Masson's trichrome staining was used to analyze the HTS tissue structure (Fig. 4B). To verify the expression of potential immune-related DEGs, we used qPCR to detect their expression in HTS and normal tissues. The results of qPCR analysis showed a significant reduction in the expression of CCL2 in the HTS tissue, whereas PLXDC2 and FOXF2 showed the opposite (Fig. 4C). Results were similar to those predicted earlier.

### 3.6. Prediction of protein structure to detect homology between human and rabbit proteins

We downloaded CCL2, PLXDC2 and FOXF2 protein sequences from NCBI. The homology of these proteins was compared between human and rabbit. We found that all the three genes showed similar protein structure predicted by AlphaFold program, and the PLXDC2 and FOXF2 expressed a higher amino acid sequence contrast score (Fig. 5A–F).

## 4. Discussion

HTS is a type of visible scar caused by abnormal wound healing secondary to dermal injury, resulting in pain, pruritus, reduced aesthetic appeal, and functional impairment [15]. Although it may be triggered by any skin injury, HTS is estimated to occur in 40%–70% of patients undergoing surgery, 90% of burn patients and 14% of patients with acne. As the second most frequent scar, HTS worsened postoperative rehabilitation in a variety of diseases [3]. HTS treatment has recently been improved by the development of laser therapy, diverse types of sutures, and radiation treatment, among other techniques [1,16]. However, fewer methods have been investigated for cutaneous scar prevention. Genetic intervention or gene therapy is an important strategy in biological treatments. Conditional control of a few key genes can be used to treat diseases to a certain extent, including cardiovascular diseases, neoplasms, cerebrovascular diseases, and autoimmune diseases [17]. ATF3 expression, for instance, has been shown to be significant in cardiovascular diseases. A few studies showed that ATF3 regulation retarded the progression of heart failure [18]. In cancer research, genetic interventions have been suggested as potential treatments for multiple cancers in chemotherapy, targeted therapy, and immunotherapy [17]. The pathophysiology of the scar formation, which is a benign tumor-like abnormal hyperplastic tissue, also involved

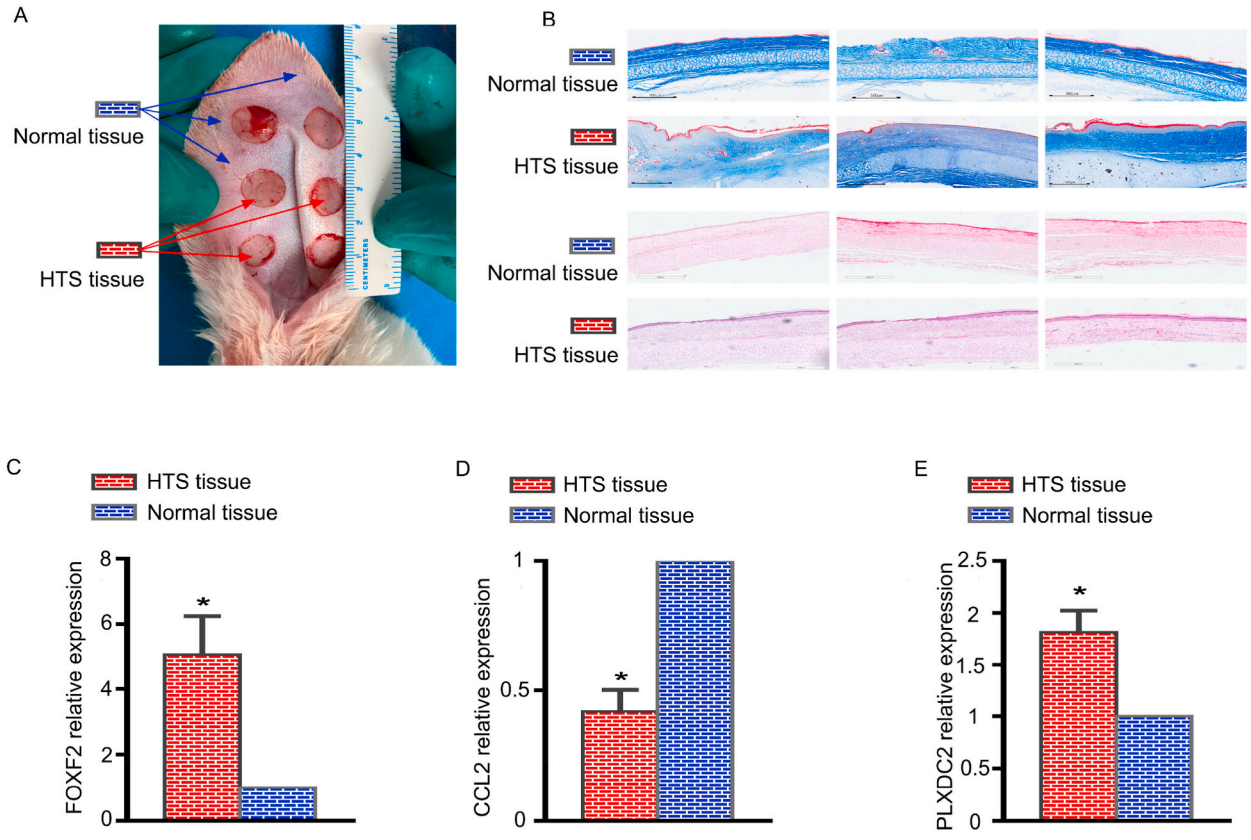


**Fig. 4.** Construction of HTS animal model and verification of the expression of potential key genes. (A) Construction of rabbit ear scar model representing HTS in animals; (B) Masson's trichrome and HE straining shows scar tissue structure; (C to E) Basic expression levels of FOXF2, CCL2 and PLXDC2 in HTS and normal tissues from the rabbit ear scar model. * means p value $< 0.05$.

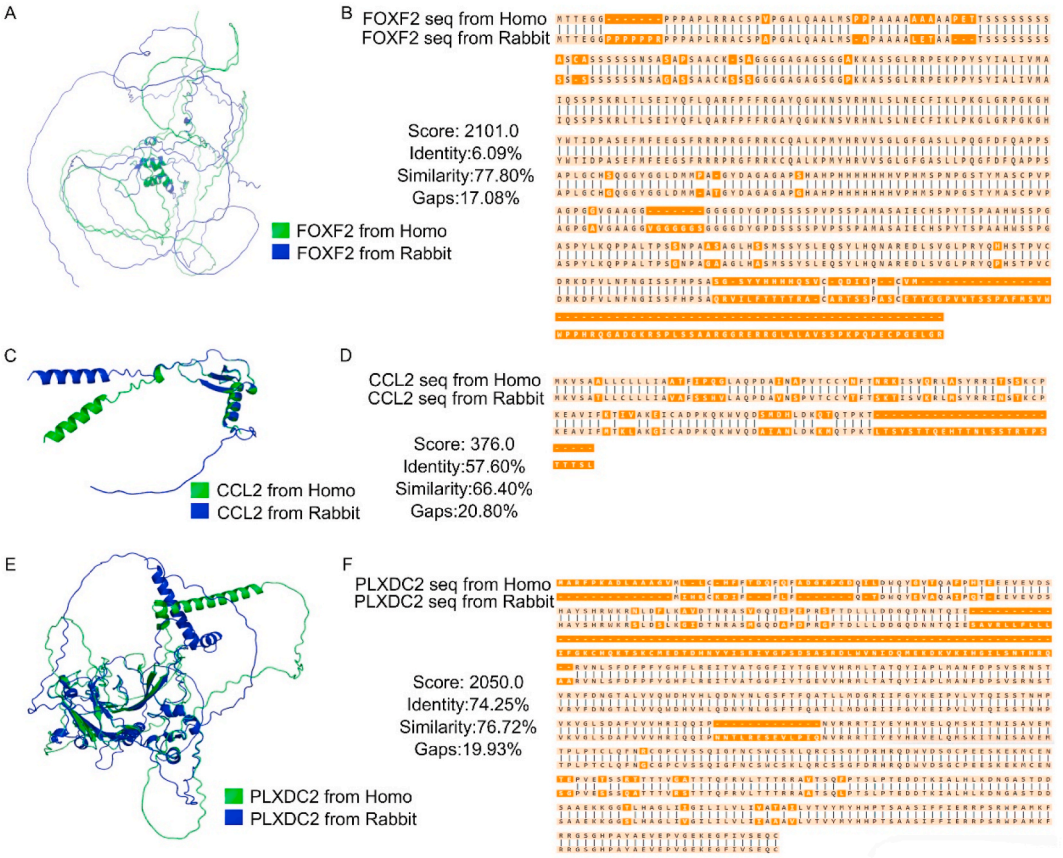


**Fig. 5.** Comparison of homology of potential key genes derived from human and rabbit cells. (A, C, and E) The protein structure was predicted and merged for homology analyses by AlphaFold; (B, D, and F) Amino acid sequence comparison shows the homology of FOXF2, CCL2, and PLXDC2 genes between human and rabbit cells, respectively.

gene regulation. Engrailed-1 is a key gene involved in scar inhibition. The activity of Engrailed-1 switched on a pro-fibrotic program in mice, whereas inhibition of its expression reversed the changes in fibrotic cells [19]. Verteporfin, which is a YAP inhibitor, has been developed and used to treat scars [20]. In this study, we identified the key genes based on HTS public data and validated our findings in the HTS animal model. Considering the close relationship between scar and immune cells, we hypothesized that the identified key genes exhibit a close relationship with at least one kind of immune cells in the scar tissues. Our results suggest that FOXF2, CCL2 and PLXDC2 may be the potential key genes in HTS tissues.

In this study, we retrieved only a single dataset associated with HTS from the GEO database and analyzed it via several bioinformatics methods. In the first step, we used edgeR to analyze the differential gene expression in pairwise comparisons between HTS and normal tissues. Twenty-two DEGs were identified in the 6 pairs of tissue samples. To further analyze the DEG signatures, GO and KEGG pathway analyses were performed using goana and kegga functions in limma. We found more than 5 DEGs focusing on cell chemotaxis, transforming growth factor beta, and cytokine-cytokine receptor interaction. A PPI network was then constructed to display the difference of gene expressions. The use of PPT network and other similar HTS studies is limited by the lack of sequencing data. Considering the important role of immune function in HTS formation and similar benign tumor-like features of HTS, a CIBERSORT analysis (to quantify specific known cell populations) was performed to assess the differential composition of immune cell infiltrates in HTS and normal tissues. The results showed that the main immune cell infiltrates in HTS included T-cell lymphomas and B-cell lymphoma cells. We also found evidence underlying the numerical correlation between immune cell infiltrates in HTS, such as CD4 T cells (memory and resting) and CD8 T cells, resting and activated NK cells, and monocytes and macrophages M0. Some of these have been previously reported and others remain to be confirmed [21–23]. We compared the differences in immune infiltrating cell composition between HTS and normal tissues. Our results suggested significant differences in the distribution of naïve B cells. In contrast to mature B cells, naive B cells do not carry the receptor for the APCs specific to their location in the bloodstream. Activation occurs when they contact with the appropriate antigen or when they become memory B cells. Some studies reported that naïve B cells also develop into short-lived plasma cells under specific scenarios [24]. It is one of the most important immune cells and accounts for more than 80% of total B cells in the immune system. In this study, the estimated naïve B-cell infiltration but not mature B cells differed statistically significantly between HTS and normal tissues, consistent with the current study findings. A proteomic study reported that naïve B cells exhibit a complex time-dependent homeostatic effect on the injured microenvironment by reducing

inflammation-associated protein expression. However, the detailed mechanisms remain elusive [25]. As its mature form, B-cell lymphocyte infiltration was mild and found in only 23% of all acne scar specimens [26]. The evolution from naïve B cell to B-cell lymphocyte and its regulatory mechanism in scar have yet to be reported. In HTS, naïve B cells may also play an important role. Its evolution may be regulated by genes and environment, and ultimately affect scar formation and development. Due to their reduced expression in HTS, we thus studied and established the relationship between naïve B cells and DEGs. The results based on this numerical statistical correlation is illustrated in Fig. 3. Six DEGs showed correlation with the number of naïve B cells, including CCL2, PLXDC2, FOXF2, CDCA7, ACKR4 and CADM1, which may be involved in the regulation of naïve B cells in HTS either as a cause or an effect.

In this study, we constructed an animal model of HTS in rabbit to verify the results of analysis. We found increasing stromal deposition and fibrosis in the rabbit HTS tissues with Masson's trichrome stain. We detected the gene expression of DEGs in the HTS and normal tissues. Three of those DEGs (FOXF2, CCL2 and PLXDC2) were differentially expressed between HTS and normal tissues. FOXF2 is a transcription factor expressed in lung and placenta to transcriptionally activate several lung-specific genes, and plays a number of roles in embryonic development [27]. The FOXF2-associated diseases include Anterior Segment Dysgenesis and Acrorenal Syndrome [28]. In most tumor types, FOXF2 is an oncogene, and knockdown of FOXF2 expression reduces cancer malignancy and inhibits angiogenesis [27]. Studies investigated CCL2 and skin healing. Complete CCL2 deficiency resulted in impaired myeloid cell recruitment and skin healing [29–31]. The other candidate key gene was PLXDC2, which coordinates the development and differentiation of nerve cells in various animals, including humans, mice, and chickens [32]. Evidence suggested that the knockdown of FOXF2, CCL2 and PLXDC2 regulates disease phenotype *in vitro* and *in vivo* [33–35]. Our results suggest potential therapeutic targets against HTS at the genetic level.

Due to the lack of human HTS cell lines or clinical tissues, we used AlphaFold and sequencing blast to predict the protein structure and compare human and rabbit proteins [36,37]. We found that they shared a similar protein-binding domain with high sequence and structural homology. The findings may serve as an important reference for the treatment of HTS in humans.

In this study, we focused on HTS, which is an important clinical issue in dermatology. Relatively few DEGs were mined from public databases using bioinformatics methods. The results were verified in an HTS model of rabbit ear. We investigated the potential influence of immune cell infiltration in the development of HTS and explored the relationship between different infiltrating immune cells and DEGs. The findings provide a reference for further understanding and treatment of HTS. Due to the limitations of technology and time, we could not conduct further comprehensive experimental validation to elucidate the underlying mechanism in cells and animal models. In future work, we plan to screen additional potential clues by multi-omics sequencing in this reported HTS model of rabbit ear, and elucidate the occurrence and development of HTS more comprehensively to identify new therapeutic methods.

## 5. Conclusion

In this study, we identified FOXF2, CCL2 and PLXDC2 as potential key genes in HTS based on bioinformatics analysis and experimental validation. They may also represent potential therapeutic targets against HTS. Our preliminary findings also demonstrated the correlation between naive B cells and potential key genes.

## Author contribution statement

Hong Cai: Conceived and designed the experiments; Performed the experiments.
Xuan Liu: Analyzed and interpreted the data.
Dingbin Liu: Contributed reagents, materials, analysis tools or data.
Bin Liu: Conceived and designed the experiments; Performed the experiments; Wrote the paper.

## Data availability statement

The authors are unable or have chosen not to specify which data has been used.

## Funding statement

National Natural Science Foundation of China (No.82274312).

## Declaration of competing interest

The authors declare that they have no known competing financial interests or personal relationships that could have appeared to influence the work reported in this paper

## References

[1] M. Hosseini, J. Brown, K. Khosrotehrani, A. Bayat, A. Shafiee, Skin biomechanics: a potential therapeutic intervention target to reduce scarring, Burns Trauma 10 (2022) tkac036.

[2] S. Amjadian, S. Moradi, P. Mohammadi, The emerging therapeutic targets for scar management: genetic and epigenetic landscapes, Skin Pharmacol. Physiol. 35 (2022) 247–265.
[3] R. Leszczynski, C.A. da Silva, Acpn Pinto, U. Kuczynski, E.M. da Silva, Laser therapy for treating hypertrophic and keloid scars, Cochrane Database Syst. Rev. 9 (2022) CD011642.
[4] L. Schaffrick, J. Ding, P. Kwan, E.E. Tredget, Molecular features of hypertrophic scars after thermal injury: is there a biologic basis for laser therapy? Adv. Wound Care (New Rochelle) 11 (2022) 163–178.
[5] R. Ogawa, The most current algorithms for the treatment and prevention of hypertrophic scars and keloids: a 2020 update of the algorithms published 10 Years ago, Plast. Reconstr. Surg. 149 (2022) 79e–94e.
[6] C. Choi, I. Mukovozov, A. Jazdarehee, R. Rai, M. Sachdeva, M. Shunmugam, K. Zaslavsky, S. Byun, B. Barankin, Management of hypertrophic scars in adults: a systematic review and meta-analysis, Australas. J. Dermatol. 63 (2022) 172–189.
[7] M.G. Fernandes, L.P. da Silva, M.T. Cerqueira, R. Ibanez, C.M. Murphy, R.L. Reis, F.J.O. Brien, A.P. Marques, Mechanomodulatory biomaterials prospects in scar prevention and treatment, Acta Biomater. 150 (2022) 22–33.
[8] B. Kuehlmann, C.A. Bonham, I. Zucal, L. Prantl, G.C. Gurtner, Mechanotransduction in wound healing and fibrosis, J. Clin. Med. 9 (2020).
[9] X. Xu, S. Gu, X. Huang, J. Ren, Y. Gu, C. Wei, X. Lian, H. Li, Y. Gao, R. Jin, B. Gu, T. Zan, Z. Wang, The role of macrophages in the formation of hypertrophic scars and keloids, Burns Trauma 8 (2020), tkaa006.
[10] P. Gal, L. Varinska, L. Faber, S. Novak, P. Szabo, P. Mitrengova, A. Mirossay, P. Mucaji, K. Smetana, How signaling molecules regulate tumor microenvironment: parallels to wound repair, Molecules 22 (2017).
[11] J. Zhang, Y. Li, X. Bai, Y. Li, J. Shi, D. Hu, Recent advances in hypertrophic scar, Histol. Histopathol. 33 (2018) 27–39.
[12] A.W. Stevenson, Z. Deng, A. Allahham, C.M. Prele, F.M. Wood, M.W. Fear, The epigenetics of keloids, Exp. Dermatol. 30 (2021) 1099–1114.
[13] D. Szklarczyk, A.L. Gable, K.C. Nastou, D. Lyon, R. Kirsch, S. Pyysalo, N.T. Doncheva, M. Legeay, T. Fang, P. Bork, L.J. Jensen, C. von Mering, The STRING database in 2021: customizable protein-protein networks, and functional characterization of user-uploaded gene/measurement sets, Nucleic Acids Res. 49 (2021) D605–D612.
[14] A.M. Newman, C.B. Steen, C.L. Liu, A.J. Gentles, A.A. Chaudhuri, F. Scherer, M.S. Khodadoust, M.S. Esfahani, B.A. Luca, D. Steiner, M. Diehn, A.A. Alizadeh, Determining cell type abundance and expression from bulk tissues with digital cytometry, Nat. Biotechnol. 37 (2019) 773–782.
[15] W.D. Short, O.O. Olutoye 2nd, B.W. Padon, U.M. Parikh, D. Colchado, H. Vangapandu, S. Shams, T. Chi, J.P. Jung, S. Balaji, Advances in non-invasive biosensing measures to monitor wound healing progression, Front. Bioeng. Biotechnol. 10 (2022), 952198.
[16] P. Kolimi, S. Narala, D. Nyavanandi, A.A.A. Youssef, N. Dudhipala, Innovative treatment strategies to accelerate wound healing: trajectory and recent advancements, Cells 11 (2022).
[17] D. Hanahan, Hallmarks of cancer: new dimensions, Cancer Discov. 12 (2022) 31–46.
[18] H. Zhou, N. Li, Y. Yuan, Y.G. Jin, H. Guo, W. Deng, Q.Z. Tang, Activating transcription factor 3 in cardiovascular diseases: a potential therapeutic target, Basic Res. Cardiol. 113 (2018) 37.
[19] S. Mascharak, H.E. desJardins-Park, M.F. Davitt, M. Griffin, M.R. Borrelli, A.L. Moore, K. Chen, B. Duoto, M. Chinta, D.S. Foster, A.H. Shen, M. Januszyk, S. H. Kwon, G. Wernig, D.C. Wan, H.P. Lorenz, G.C. Gurtner, M.T. Longaker, Preventing Engrailed-1 activation in fibroblasts yields wound regeneration without scarring, Science (2021) 372.
[20] N. Gao, L. Lu, X. Ma, Z. Liu, S. Yang, G. Han, Targeted inhibition of YAP/TAZ alters the biological behaviours of keloid fibroblasts, Exp. Dermatol. 31 (2022) 320–329.
[21] H. Zhang, S. Cao, Y. Xu, X. Sun, M. Fei, Q. Jing, X. Xu, J. Tang, B. Niu, C. Li, Landscape of immune infiltration in entorhinal cortex of patients with Alzheimer's disease, Front. Pharmacol. 13 (2022), 941656.
[22] M. Gryziak, K. Wozniak, L. Kraj, L. Rog, R. Stec, The immune landscape of hepatocellular carcinoma-where we are? Oncol. Lett. 24 (2022) 410.
[23] W. Fu, G. Ma, Significance of immunogenic cell death-related genes in prognosis prediction and immune microenvironment landscape of patients with cutaneous melanoma, Front. Genet. 13 (2022), 988821.
[24] A. Goretzki, Y.J. Lin, C. Meier, B. Dorn, S. Wolfheimer, A. Jamin, M. Schott, A. Wangorsch, S. Vieths, T. Jakob, S. Scheurer, S. Schulke, Stimulation of naive B cells with a fusion protein consisting of FlaA and Bet v 1 induces regulatory B cells ex vivo, Allergy 78 (3) (2023 Mar) 663–681.
[25] R.F. Sîrbulescu, A. Mamidi, S.C. Chan, G. Jin, M. Boukhali, D. Sobell, I. Ilieş, J.Y. Chung, W. Haas, M.J. Whalen, A.E. Sluder, M.C. Poznansky, B cells support the repair of injured tissues by adopting MyD88-dependent regulatory functions and phenotype, FASEB J 35 (12) (2021), e22019.
[26] B. Chancheewa, P. Asawanonda, N. Noppakun, C. Kumtornrut, Myofibroblasts, B cells, and mast cells in different types of long-standing acne scars, Skin Appendage Disord. 8 (6) (2022) 469–475, https://doi.org/10.1159/000524566. Epub 2022 May 12. PMID: 36407643; PMCID: PMC9672862.
[27] W. He, Y. Kang, W. Zhu, B. Zhou, X. Jiang, C. Ren, W. Guo, FOXF2 acts as a crucial molecule in tumours and embryonic development, Cell Death Dis. 11 (2020) 424.
[28] L.M. Reis, R.C. Tyler, B.A. Volkmann Kloss, K.F. Schilter, A.V. Levin, R.B. Lowry, P.J. Zwijnenburg, E. Stroh, U. Broeckel, J.C. Murray, E.V. Semina, PITX2 and FOXC1 spectrum of mutations in ocular syndromes, Eur. J. Hum. Genet. 20 (2012) 1224–1233.
[29] J. Pang, M. Maienschein-Cline, T.J. Koh, Enhanced proliferation of Ly6C(+) monocytes/macrophages contributes to chronic inflammation in skin wounds of diabetic mice, J. Immunol. (Baltimore, Md : 1950) 206 (2021) 621–630.
[30] A. Villarreal-Ponce, M.W. Tiruneh, J. Lee, C.F. Guerrero-Juarez, J. Kuhn, J.A. David, K. Dammeyer, R. Mc Kell, J. Kwong, P.S. Rabbani, Q. Nie, D.J. Ceradini, Keratinocyte-Macrophage crosstalk by the Nrf2/Ccl2/EGF signaling Axis orchestrates tissue repair, Cell Rep. 33 (2020), 108417.
[31] Y. Mizutani, A. Kanbe, H. Ito, M. Seishima, Activation of STING signaling accelerates skin wound healing, J. Dermatol. Sci. 97 (2020) 21–29.
[32] M.T. Deng, F. Zhu, Y.Z. Yang, F.X. Yang, J.P. Hao, S.R. Chen, Z.C. Hou, Genome-wide association study reveals novel loci associated with body size and carcass yields in Pekin ducks, BMC Genom. 20 (2019) 1.
[33] A.D. Talsma, J.P. Niemi, J.S. Pachter, R.E. Zigmond, The primary macrophage chemokine, CCL2, is not necessary after a peripheral nerve injury for macrophage recruitment and activation or for conditioning lesion enhanced peripheral regeneration, J. Neuroinflammation 19 (2022) 179.
[34] B. Wu, Y.X. Wang, J.J. Wang, D.F. Xiang, M.S. Zhang, Z.X. Yan, W.Y. Wang, J.Y. Miao, X. Lan, J.J. Liu, Z.Y. Li, C. Li, J.Y. Fan, J.Y. Liu, L. Jiang, S.L. Xu, Y.H. Cui, F. Qian, PLXDC2 enhances invadopodium formation to promote invasion and metastasis of gastric cancer cells via interacting with PTP1B, Clin. Exp. Metastasis 39 (2022) 691–710.
[35] B.P. Herring, A.M. Hoggatt, A. Gupta, J.M. Wo, Gastroparesis is associated with decreased FOXF1 and FOXF2 in humans, and loss of FOXF1 and FOXF2 results in gastroparesis in mice, Neuro Gastroenterol. Motil. 31 (2019), e13528.
[36] R. Nussinov, M. Zhang, Y. Liu, Jang H. AlphaFold, Artificial intelligence (AI), and allostery, J. Phys. Chem. B 126 (2022) 6372–6383.
[37] D.V. Laurents, AlphaFold 2 and NMR spectroscopy: partners to understand protein structure, dynamics and function, Front. Mol. Biosci. 9 (2022), 906437.